ACS APPLIED MATERIALS & INTERFACES

Research Article

www.acsami.org

High-Rate and High-Energy-Density Lithium-Ion Battery Anode Containing 2D MoS_2 Nanowall and Cellulose Binder

Uttam Kumar Sen and Sagar Mitra*

Electrochemical Energy Laboratory, Department of Energy Science and Engineering, Indian Institute of Technology, Bombay, Mumbai-400076, India

Supporting Information

ABSTRACT: Electrochemically stable molybdenum disulfide (MoS_2) with a two-dimensional nanowall structure is successfully prepared by a simple two-step synthesis method followed by thermal annealing at 700 °C in a reducing atmosphere. MoS_2 nanowalls provide a better electrochemical performance and stability when cellulose (CMC) binder is used instead of the usual PVDF. The electrodes exhibit a high specific discharge capacity of 880 mA h g^{-1} at 100 mA g^{-1} without any capacity fading for over 50 cycles. The electrode also exhibits outstanding rate capability with a reversible capacity as high as 737 mA h g^{-1} and 676 mA h g^{-1} at rates of 500 mA g^{-1} and 1000 mA g^{-1} at 20 °C, respectively. The excellent electrochemical stability and high specific capacity of the nano structured materials are attributed to the two-dimensional nanowall morphology of MoS_2 and the use of cellulose binder. These results are the first of its kind to report a superior stability using bare MoS_2 as an active material and CMC as a binder.

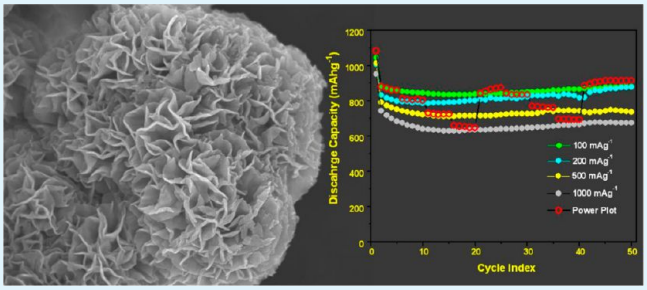

KEYWORDS: *2D- MoS_2 nanowalls, CMC binder, high power density anode, hydrothermal synthesis, lithium-ion battery*

INTRODUCTION

An increase in environmental toxicity, climate change, and an energy shortage are urgent issues that are important to all nations. Considering the particular importance of the energy crisis, this project seeks to exploit a new class of materials or devices to significantly increase our ability to produce clean electricity for portable instruments and the grid. Electrochemical energy storage is considered as one of the identified solutions to provide or to support clean electricity.

Our current interest focuses on the rechargeable Li-ion battery application as a possible solution to provide a clean storage option for portable instruments and the grid. Hence, we address a few issues or requirements related to energy, power, stability, and safety of current lithium-ion battery. Most of the current lithium-ion battery electrode materials suffer from stability, safety, and capacity issues at high rate, which restricts its use for next-generation battery applications in its current status. To overcome these problems, a new class of cost-effective, low-dimensional layered materials has been introduced in the literature.[1−7] Among them molybdenum disulfide (MoS_2) has received much attention in particular because it can accommodate lithium ions at lower potential through conversion reaction and hence it can be used as anode paired with a suitable high voltage (>4 V) lithiated cathode.[8] MoS_2 reacts with lithium ions namely by conversion mechanism, forming Mo nanoparticles and insoluble Li_2S matrix. The outcome of this conversion reaction leads to four moles of lithium incorporation per mole of MoS_2 which accounts for 670 mA h g^{-1} lithium storage capacity, one and half time higher than current graphite anode.

Besides the huge capacity gain, the conversion reaction suffers from electrolyte decomposition catalyzed by Li_2S, leading to a rise in the formation of a thick polymeric layer resulting in poor cyclic stability, rate capability, and first cycle irreversible capacity loss.[8] By adopting various carbon coating techniques, many researchers had improved the stability as well as rate capability of MoS_2 as anode material.[9−11] On the contrary, the bare MoS_2 still suffers from electrochemical instability and poor cyclic performance. Nanostructuring of anode materials along with the use of new binder can help overcome the difficulties associated with conversion reaction and envision a better conversion electrode. The choice of new binder could be cellulose (CMC), which exhibits a strong interaction between conversion anodes and facilitates the reaction processes by overcoming the mechanical issues associated with the huge volume expansion. The selection of new binder like CMC over PVDF is a logical choice for the conversion reaction as it has been reported earlier that CMC binder shows better stability in comparison to PVDF in case of alloying reaction where huge volume change is accounted due to incorporation of large amount of Li in the matrix.[12,13] In commercial Li-ion battery electrode, materials like carbon and $LiCoO_2$ mixed with PVDF binder exhibit excellent cyclic

Received: October 3, 2012
Accepted: January 28, 2013
Published: January 28, 2013

Scheme 1. Schematic of the Reaction Setup and the Progress of the Reaction

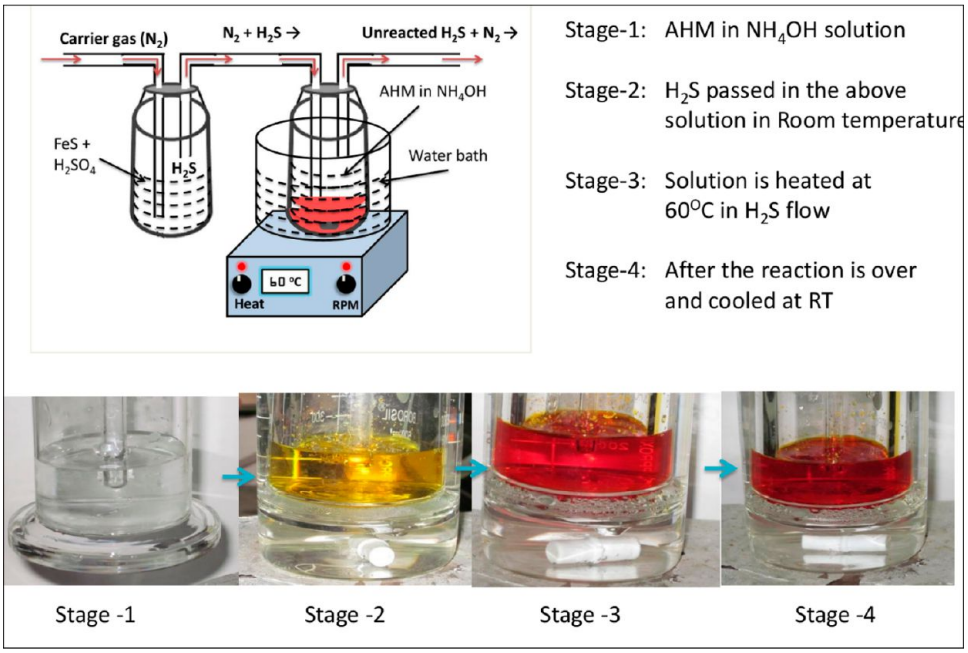

performance as they undergo relatively small volume changes (12 and 6%, respectively).[12]

Our belief at this point is that the combination of MoS_2 and CMC binder could successfully overcome the effect of volume change and improve the electrochemical performance with excellent cycling stability and rate capability. Herein, we have used a simple cost-effective chemistry to produce MoS_2 nanomaterial to be used as lithium battery anode. A carbon free MoS_2-nano material has demonstrated a superior cyclic stability using CMC (sodium salt of carboxy methyl cellulose) as a binder. MoS_2 nanomaterial shows a stable capacity of 880 mA h g^{-1} for 50 cycles at a current rate of 100 mA g^{-1}, whereas the same material exhibits a stable capacity of 676 mA h g^{-1} when discharged at 1000 mA g^{-1}. The current rate capability can be considered as one of the best performances of MoS_2 in the literature.

EXPERIMENTAL SECTION

Preparation of MoS_2 Nanowalls. MoS_2 nanowalls was prepared by a two step synthesis process. The detailed experimental process is illustrated in Scheme 1. All the precursors were used, as received, without further treatment. Typically, 5 g of ammonium hepta-molybdenum (AHM) (99%, Merck, India) was dissolved in 10 mL of deionized water by stirring; 35 mL of ammonium hydroxide (30%, Merck, India) was added to it and stirred to make a clear solution. H_2S gas was then passed into the solution. Initially H_2S was passed vigorously into the solution at room temperature (30 °C) to saturate the solution with H_2S. The reaction setup was then placed in a water bath kept at 60 °C with controlled flow of H_2S for 30 min. During the reaction, the color of the solution changed from colorless to pale yellow to orange. As the color of the solution turned orange, the H_2S flow was stopped and the solution was kept at room temperature for a couple of hours. A deep orange color solution was obtained, which was transferred to a 100 mL Teflon-lined autoclave and placed inside a muffle furnace at 180 °C for 24 h. Black color precipitation obtained at the end of the hydrothermal treatment, was filtered, washed, and dried in hot air oven at 60 °C for 12 h and finally annealed at 700 °C for 4 h in reducing atmosphere (5% H_2 balanced with N_2).

Characterizations. Material characterization was done by powder X-ray diffraction (XRD) measurements at room temperature (30 °C) using a Philips X'-pert diffractometer with Cu Kα radiation (λ = 1.5418 Å) at 40 kV and 40 mA. Different metal−sulfur vibration nodes were obtained using a Raman spectrometer (Jobin Yvon HR800) having 514.5 nm laser at 10 mW power. A field-emission gun scanning electron microscope (FEG-SEM, JEOL-7600F) with a resolution of about 1 nm was used to study the surface morphology of the samples. Further investigations were done by the use of high resolution field emission transmission electron microscope (HR-TEM, JEOL-2100F). For SEM analysis, powder sample was sprinkled over carbon film and images were taken at the best operating condition. For TEM analysis, a well-dispersed solution was prepared by adding a little amount of MoS_2 powder in acetone and sonicating it for 10−15 min. One drop of the dispersed solution was taken on the TEM grid to obtain images at the best operating condition.

Cell Fabrication and Electrochemical Measurements. Galvanostatic charge−discharge test was carried out in CR2032 coin cells having a cell configuration of Li/Electrolyte/MoS_2. Cells were assembled in an argon-filled glovebox (Lab Star, Mbraun, Germany) with moisture and oxygen concentration level of ∼1 ppm. Lithium foil was used as the counter as well as reference electrode and 1 M $LiPF_6$ in EC/DMC (1:1 vol./vol.) (LP-30, Merck, Germany) as the electrolyte. Borosilicate glass microfiber filters (Whatman) were used as a separator. The electrodes were prepared using MoS_2 as the active material, carbon black (Super C-65, Timcal, Switzerland) as the conductive substance, and a polymeric binder (CMC) with an overall ratio of 3:1:1 (by wt). To get a better understanding of the electrochemical performance, we prepared three different electrodes using the same active material and same weight ratio of carbon. First electrode (I) was prepared by using MoS_2 annealed with C and then added to CMC (Lobachemie, India). Second electrode (II) was prepared using MoS_2 annealed without C, which was then mixed with carbon and CMC. The third electrode (III) was prepared in the same way as electrode (I); however, PVDF (Sigma Aldrich) was used instead of CMC. Slurry was prepared by adding few drops of deionized water for electrode (I) and (II), i.e., in the case of CMC binder, whereas NMP (Qualigens, India) was used for electrode (III), i.e., for PVDF with the help of a constant stirring for 2 h at 30 °C. This slurry was then cast on Cu foil using doctor's blade and the electrode was dried at 60 °C under vacuum for 12 h and pressed. Cyclic voltammetry (CV) profile was obtained by measuring $i-V$ response at scan rate of 0.2 mV s^{-1} within the potential window of 0.01−3.0 V, using Biologic VMP-3. The electrochemical charge−discharge was performed using

Arbin Instrument, USA (BT2000 model) at various constant current rates. All the electrochemical measurements were done at a constant temperature of 20 °C.

RESULTS AND DISCUSSION

Structural Characterization. A step synthesis processes were used to produce MoS_2 nanowalls. In the first step, an orange color solution was obtained is due to the formation of ammonium tetrathiomolybdate $\{(NH_4)_2MoS_4\}$.[14] The orange color $(NH_4)_2MoS_4$ solution decomposed during the hydrothermal treatment to form black color MoS_2. The balanced equation for decomposition reaction is given below

$$(NH_4)_2MoS_4 \rightarrow MoS_2 + 2NH_3 \uparrow + 2H_2S\uparrow$$

XRD pattern of MoS_2 powder is shown in Figure 1a, which is indexed as orthorhombic phase of MoS_2 (JCPDS card No. 37−1492). Raman analysis shown in Figure 1b also confirms the formation of MoS_2 pure phase. MoS_2 exhibits sharp peaks at 384 cm^{-1} (E^1_{2g}) and 408 cm^{-1} (A_{1g}) that are due to the first-order Raman vibration modes within the S−Mo−S layer.[15,16]

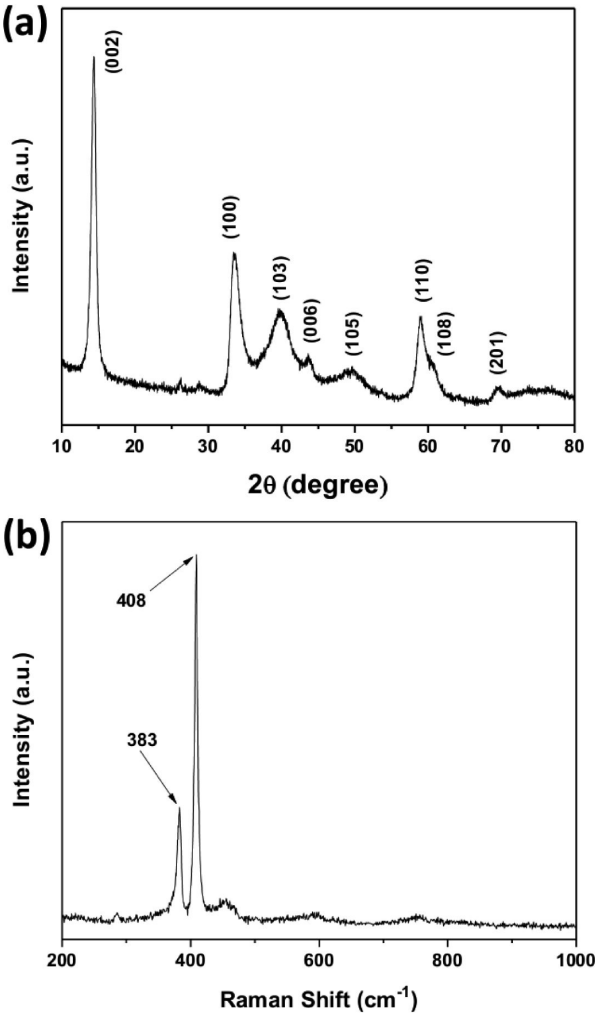

Figure 1. (a) XRD and (b) Raman spectra of annealed MoS_2.

High-resolution scanning electron microscopy was used to study the morphology of the MoS_2. FEG-SEM images (shown in Figure 2a, b) illustrates that flake/wall type morphology of MoS_2 obtained, has agglomerated to form cauliflower morphology.

FEG-SEM analysis shows uniformity in the morphology with wall thickness in the range of 19−23 nm. FEG-TEM gives a better look on an isolated MoS_2 nanowall (Figure 2c). The agglomerated cauliflower is not visible in FEG-TEM images, as during the FEG-TEM sample preparation the powder sample was ultrasonically dispersed in acetone which caused the separation of MoS_2 flakes, whereas direct powder samples was used for SEM analysis. The high resolution images (Figure 2d, e) identify that the well-defined layered structures of MoS_2 having an interlayer distance of 0.62 nm for (200) planes[17] has been observed.

From different morphological analysis, the plausible growth mechanism of cauliflowerlike MoS_2 formation has been illustrated in Scheme 2. At the initial stage of the reaction, $(NH_4)_2MoS_4$ decomposed to form MoS_2 nanosheets.[8] As the reaction medium is highly basic, excess of OH^- ions were present in the solution which is known to have blocking effect on ⟨001⟩ direction to form a lamellar structure.[18] As a result, growth of MoS_2 occurred in two directions only to form nanosheets. The monolayered or bilayered MoS_2 nanosheets were attached to each other by van der Waal interaction and finally self-assembled to form MoS_2 nano wall/flake. From the HR-TEM analysis, it is clearly observed that each MoS_2 nano wall/flake consists of thin MoS_2 nanosheets. The stacking of nanosheets into nanowall is driven by the thermodynamics to minimize the surface energy.[19] Stacking of nanosheets into nano walls/flakes were also observed by other work reported in the literature.[20,21] Finally the nanowalls were agglomerated during precipitation to form cauliflowerlike MoS_2. The anisotropy in the cauliflowerlike morphology (shown in Figure S1 in the Supporting Information) proves that it is agglomeration rather than central nucleation (where the flakes are growing from a common point at the center of the cauliflower ball) that leads to the final morphology. The effect of thermal annealing on the morphology was also checked which shows that there was no change in the morphology due to thermal annealing which again implies that cauliflowerlike morphology was already formed during hydrothermal synthesis. FEG-SEM images were taken before and after thermal annealing at 700 °C are shown in Figure S2 of the Supporting Information.

Electrochemical Performance. As mentioned earlier, three different electrodes were prepared to check the electrochemical activity of MoS_2 nanowalls. Electrode (I) and (II) were prepared by using CMC whereas electrode (III) was prepared the same way as electrode (I) but instead of CMC, PVDF was used.

XRD analysis of three different thermal treatment conditions is shown in Figure 3,which reveals that the presence of carbon during calcination of MoS_2 does not affect the crystallization process as the position of the diffraction peaks and their relative intensities remain same as in case of pure MoS_2. Figure 3 also shows that mixed carbon is graphitized when preheated at 700 °C. The graphitized carbon leads to a better electron percolation inside the electrode material, which causes the enhancement of the electrochemical performance of the active material (discussed later).

Cyclic voltammogram (CV) of electrode (I), (II), and (III) are shown in Figure 4. During the first discharge process of electrode (I), two prominent peaks were observed at 0.9 and 0.3 V vs Li/Li^+. The peak at 0.9 V is due to the intercalation of Li^+ in the interlayer spacing of MoS_2 (formation of Li_xMoS_2), whereas the peak at 0.3 V is the characteristics of Li_xMoS_2 to

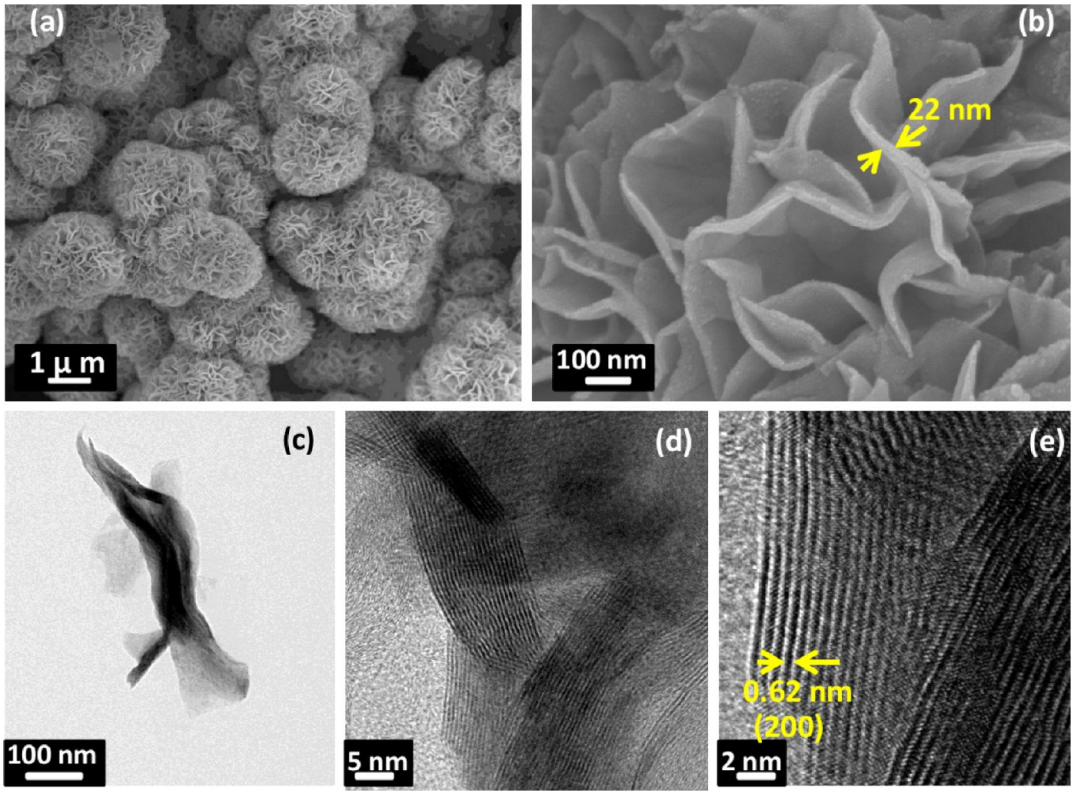

Figure 2. (a, b) FEG-SEM and (c–e) FEG-TEM images of MoS_2 nanowall morphology.

Scheme 2. Schematic Representation for the Growth Mechanism of Cauliflowerlike MoS_2

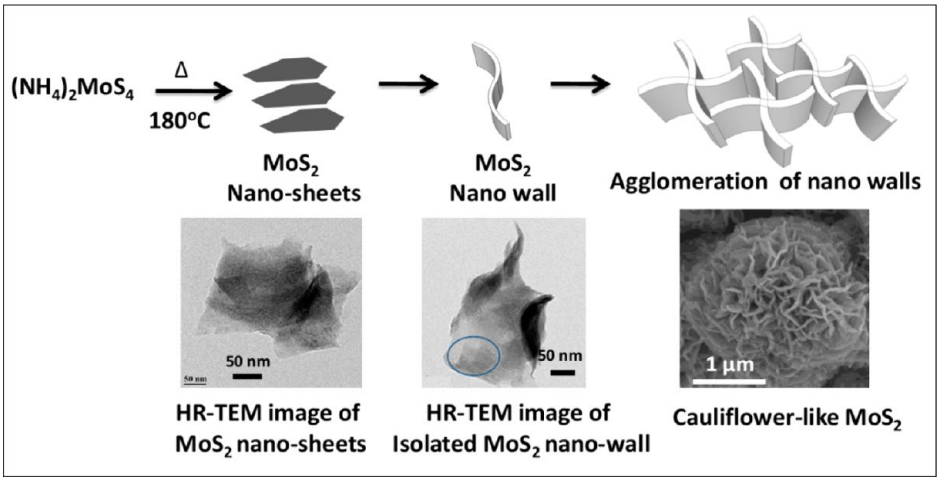

L_2S + Mo/Li_y conversion reaction. The discharge capacity corresponding to first lithium insertion into MoS_2 lattice (shown in Figure 5a, later) is about 300 mA h g^{-1}, corresponding of 1.8 lithium insertion per formula unit of MoS_2 (theoretically, 167 mA h g^{-1} is equivalent to one lithium intake per formula unit of MoS_2). Moreover, we have assumed here that Li solubility is minimum in Mo and there has been a very little chance to form Mo–Li alloy. Interestingly, before starting the sharp conversion reaction at 0.3 V, a broad shoulder started from 0.65 V, which signifies the starting point of the conversion reaction (as shown in the discharge curve explained latter in Figure 5b), whereas the actual peak position here is 0.3 V and shifting to lower potential in consecutive cycles due to continuous change of electronic environment. This phenomena could be explained by lithium insertion in MoS_2 layered structure, or in the defect sites of MoS_2 crystal structure together with conversion reaction.[22−24] In the anodic sweep two broad peaks at 1.5 and 1.7 V vs Li/Li^+ and a sharp peak at 2.4 V vs Li/Li^+ were observed. The dual peaks at 1.5 and 1.7 V could be associated with two-step Li-ion removal from Mo via reduction and at 2.4 V vs Li/Li^+ is due to oxidation of Li_2S into sulfur.[22]

Therefore, after completion of first cycle, the electrode comprises unreacted MoS_2, Mo, Li, and S. In the consecutive cycles, one extra peak at 1.8 V vs Li/Li^+ was observed during cathodic sweeps, which was not there in the first cycle. After careful observation, the broad peak at 1.8 V reveals that the broad peak designated for multi steps reaction mechanism of

dx.doi.org/10.1021/am3022015 | ACS Appl. Mater. Interfaces 2013, 5, 1240−1247

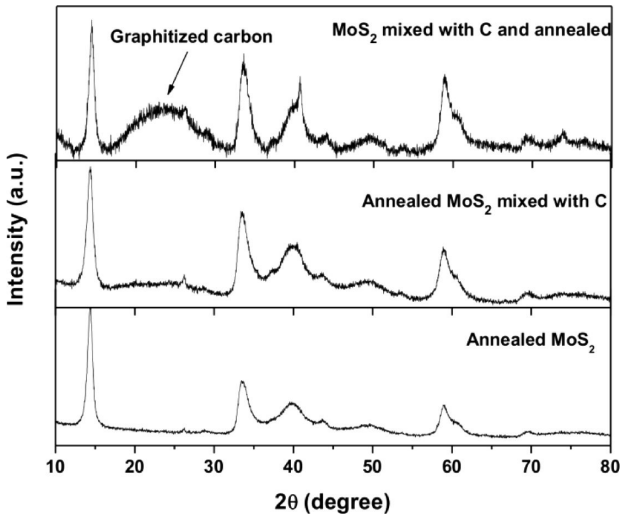

Figure 3. XRD of MoS_2 nanowall annealed with carbon and without carbon.

elemental sulfur with lithium and finally forming Li_2S.[22,25] From the consecutive CV cycles, it is revealed that this reduction peak at 1.8 V shifted to higher energy side and splits into two parts occurring at 1.9 and 2.1 V, respectively, which agrees well with the kinetics of the multistep conversion from elemental sulfur to polysulfides and then to Li_2S. It is also noteworthy to mention here that the transition between Li_2S and S is greatly influenced by the nano characteristics of Mo metal in the matrix and modifies the reaction chemistry greatly other than presence of sulfur alone. The other two catholic peaks at 1.0 V and 0.3 V vs Li/Li^+ are attributed to Li-ion insertion in defects sites and Li association with Mo, respectively.

From the cyclic voltammograms, we can say that for the electrode (I), the intensity of both these peaks are quite stable compare to other two electrodes. It has also been observed that the electrochemistry of other two electrodes (II and III) were similar to that of electrode (I) but the peak intensity constantly decrease with cycle numbers for electrode (II) and (III), which also reflects in the cyclic performance shown later.

Rate and Cyclic Performance. A comparative cyclic stability of these three electrodes is shown in Figure 4d. First discharge capacity for the three electrodes obtained at a current rate of 200 mA g^{-1} were 1008 mA h g^{-1}, 942 mA h g^{-1} and 928 mA h $g^{-1}$for electrode (I), (II), (III) respectively. Electrode (I) exhibits better electrochemical stability for 50 cycles compare to others. At the end of 50 cycles, discharge capacity exhibited by these three electrodes were 880 mA h g^{-1}, 540 mA h $g^{-1}$and 298 mAh g^{-1} which is equivalent to the capacity retention of 85, 57, and 32% (with respect to first cycle) for electrode (I), (II), and (III), respectively. So it is clearly observed that electrode (I) demonstrates a better electrochemical stability with a capacity retention of 85% when CMC is used as binder, whereas the electrode prepared using PVDF binder exhibits poor electrochemical performance with a capacity retention of

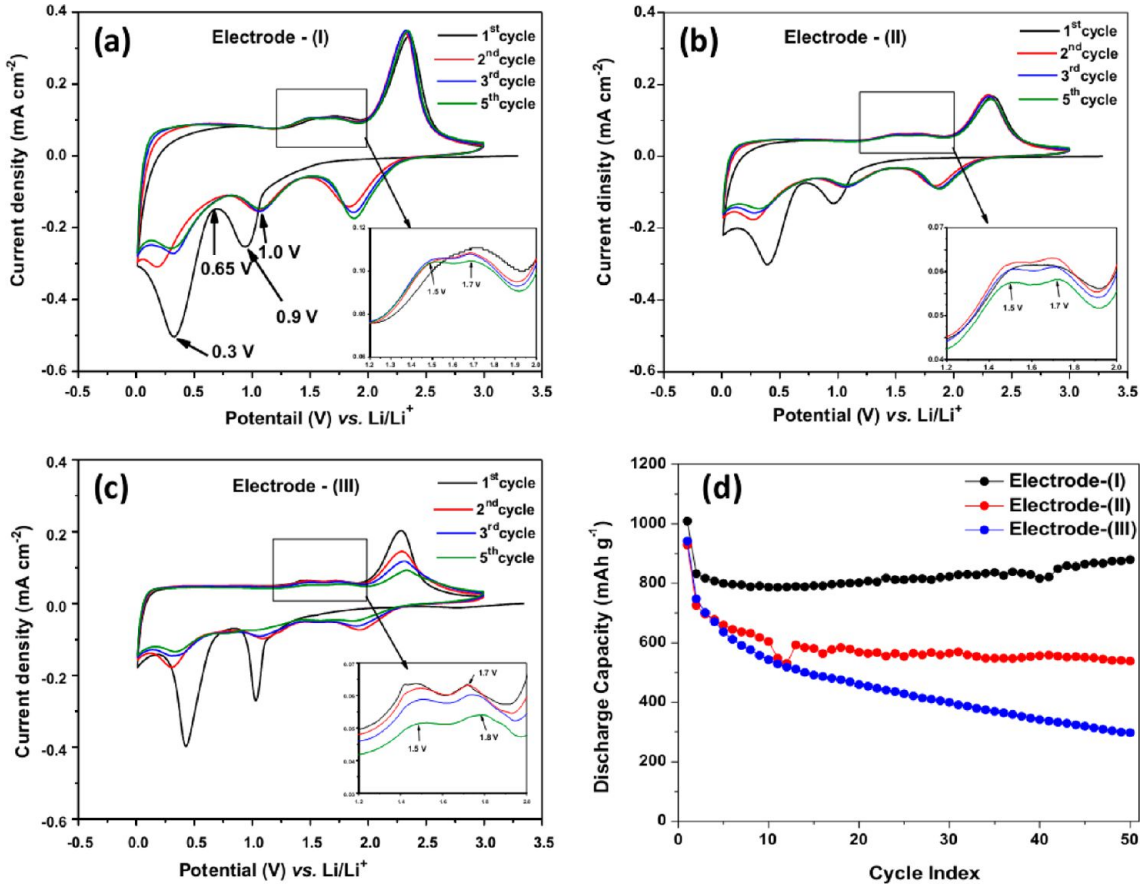

Figure 4. Cyclic voltammograms of (a) electrode (I), (b) electrode (II), and (c) electrode (III) at a scan rate of 0.2 mV s^{-1} for potential range of 3.0 to 0.01 V vs Li/Li^+. (d) Cyclic performance of electrode (I), (II), and (III) at 200 mA g^{-1} for the potential window of 3.0−0.01 V vs Li/Li^+ at 20 °C.

dx.doi.org/10.1021/am3022015 | ACS Appl. Mater. Interfaces 2013, 5, 1240−1247

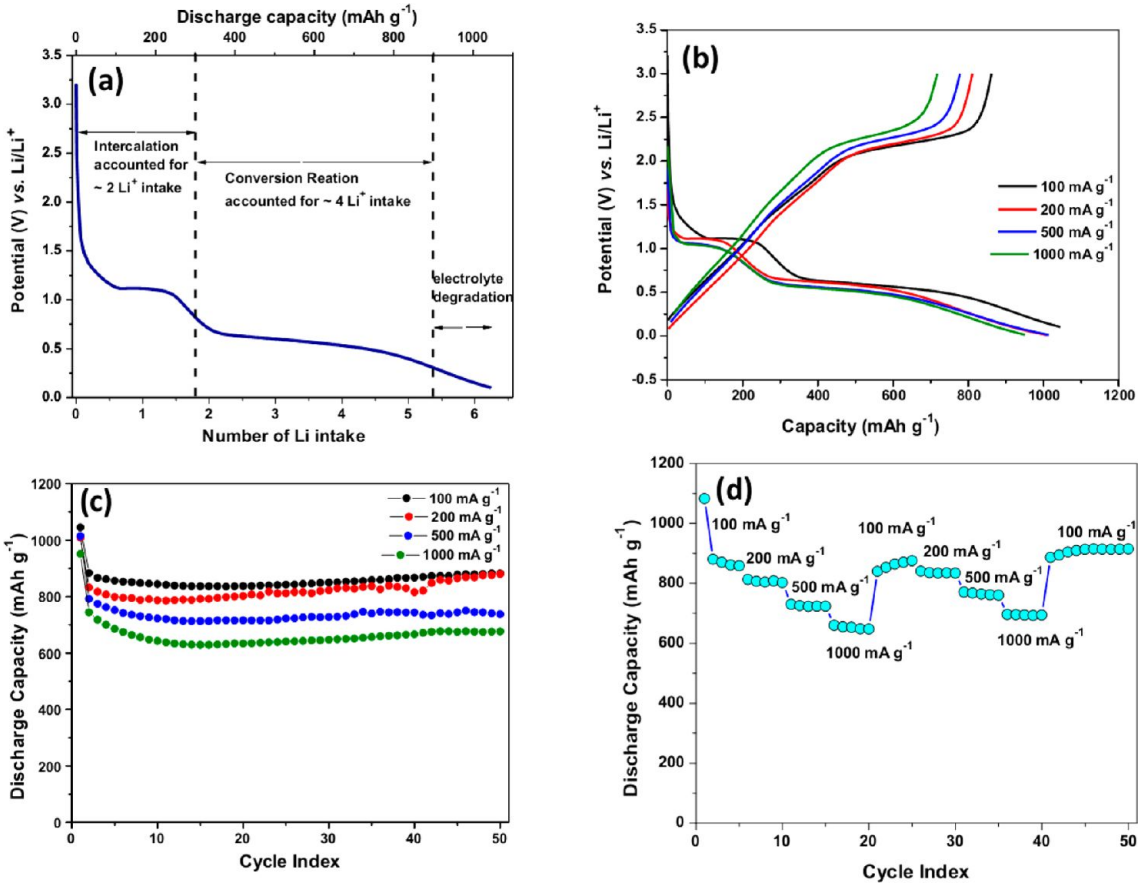

Figure 5. (a) Illustration of 1st discharge profile for electrode (I) at 100 mA g^{-1} (OCV to 0.1 V), (b) 1st discharge and charge profile (OCV to 0.01 V) of electrode (I) at different current rates at 20 °C (for 100 mA g^{-1}, it is OCV to 0.1 V), (c) cyclic performance of electrode (I) at different current rates, and (d) power cycle performance of electrode (I).

32% of the initial capacity, after 50 cycles. A comparison between MoS_2 nanowalls and commercially available bulk MoS_2 was also performed and shown in Figure S3 in the Supporting Information. Because of the mesoporous nature of MoS_2 nanowalls, it provides better initial capacity as well as better capacity retention in compare to bulk MoS_2 with same operating condition. The capacity retention for bulk MoS_2 was 63% of its initial capacity in compare to 85% for MoS_2 nanowalls. The superiority of the CMC binder over PVDF is due to the fact that CMC provides a unique homogeneous three-dimensional networking between the particles of conductive carbon and active material which leads to a better electrode architecture.[26] It assumed that the mechanical property of binder is not the only factor that influences the material performance toward the volume change.[27] The presence of polar functional groups in CMC provides effective chemical bonding with the active material as well as current collector, which enhance the stability of the electrode during cycling.[28,29] So the mechanical as well as the chemical properties of the CMC binder provide better stability to the electrode material, which leads to enhanced lithium storage capability.

The superior stability of electrode (I) may be attributed to better sintering of MoS_2 and carbon when heated at 700 °C. Because of graphitization of carbon, the electrode conductivity has been increases (impedance spectroscopy of electrode (I) & (II) shown in Figure S4 in the Supporting Information), which leads to a better performance. As a known fact of material diffusion during high temperature heating (which is widely used in semiconductor doping),[30,31] there could be a possibility of partial diffusion of carbon into the MoS_2 layers, which provide better binding between MoS_2 and carbon, leading to a better contact between the conductive carbon and active material. In other cases, where MoS_2 was first calcined and then grinded with carbon, the attachment among active material and conductive carbon is not strong enough, which leads to a loss in the electronic contact for some of the MoS_2 particles, resulting in capacity fading. To establish the superior electrochemical activity of MoS_2, we have checked the cycling performance of electrode (I) at different current rates. First discharge profile of the electrode (I) from OCV to 0.1 V vs Li/Li^+ at 100 mA g^{-1} was represented in the Figure 5a. Two distinct plateau at 1.1 and 0.6 V vs Li/Li^+ were observed respectively. The plateau at 1.1 V is due to the intercalation of Li^+ ion in the interlayer spacing of MoS_2 that accounted for ~1.8 Li^+ intake. The plateau at 0.6 V is due to conversion reaction which takes about ~4 Li^+ ion. So, almost 6 Li^+ ions per MoS_2 are accommodated in the first discharge process and exhibited discharge capacity of about 1047 mAh g^{-1} at current density of 100 mA g^{-1}. Quantitatively, 62% of the discharge capacity is contributed from conversion reaction whereas only 24% is added from intercalation reaction and the remaining 14% comes from electrolyte decomposition and/or other side reactions. Figure 5b depicts the first discharge and charge profile of same electrode (I) at different current densities. Two stable plateaus at 1.1 and 0.6 V vs Li/Li^+ were observed during

the first discharge process whereas one plateau at 2.3 V was observed during first charge process for all the current rates. Electrode (I) exhibits excellent cyclic stability as well as good discharge capacity at low as well as high current rates which is shown in Figure 5c. At a low current rate of 100 mA g^{-1}, the MoS_2 shows highly stable electrochemical performance for the span of 50 cycles with a superior discharge capacity as high as 880 mA h g^{-1} at the end of 50 cycles. At higher rate, the electrode material records proficient cyclic stability and good discharge capacity of 737 mA h g^{-1} and 676 mAh g^{-1} after 50 cycles at a discharge current rate of 500 mA g^{-1} and 1000 mA g^{-1}, respectively. Total 84% of the initial capacity was retained after 50 cycles when discharge at 100 mA g^{-1} whereas the capacity retention at high rate performances were 73 and 71% at a current rates of 500 mA g^{-1} and 1000 mA g^{-1} respectively which is an outstanding example of conversion electrode. Power cycle performance has been performed at various current rates to demonstrate the excellent electrochemical stability and robustness of the electrode material. Figure 5d shows that the material exhibits discharge capacity of 870, 804, 723, and 653 mA h g^{-1} capacity at a current rate of 100, 200, 500, and 1000 mA g^{-1}. After reversing back to the current rate of 100 mA g^{-1}, the material exhibits specific capacity of 864 mA h g^{-1} at 25th cycle.

A better mixing of MoS_2 nanowalls, carbon, and CMC binder exhibits better performance of the electrode when tested as anode material against lithium metal. Although most of the reported results on bare MoS_2 suffers fast capacity fading, our work on MoS_2 nanowalls demonstrates a stable discharge capacity of 880 mA h g^{-1} at the end of 50 cycles at a current rate of 200 mA h g^{-1}, is among the best result in this category. For example, Du et al.[32] reported 800 mA h g^{-1} stable capacity using reed MoS_2 for 50 cycles at 50 mA g^{-1}, Fenget al.[33] reported MoS_2 nanotubes were exhibiting a discharge capacity of around 790 mA h g^{-1} after 40 cycles at a current rate of 40 mA g^{-1}. Similarly, Xiao et al.[34] has reported a constant capacity of 900 mA h g^{-1} using exfoliated MoS_2 with PEO, at a current rate of 50 mA g^{-1}. Mesoporous $MoS_2$was reported by Liu et al.,[17] which exhibits a constant capacity of 876 mA h g^{-1} for 100 cycles at 100 mA h g^{-1}. Das et al.[8] reports a stable capacity of 750 mA h g^{-1} at 100 mA g^{-1} after 100 cycles using MoS_2 nanosheets. Ding et al.[35] reports MoS_2 nanosheet microspheres showing a specific capacity of 600 mA h g^{-1} after 70 cycles at a current density of 100 mA g^{-1}. Zhou et al.[36] observed a capacity of 600 mA h g^{-1}at the end of 100 cycle by using MoS_2−CMK-3 composites while discharge at 250 mA g^{-1}. Therefore, the results obtained in the present work stands ahead than most of the reported results on in situ carbon free MoS_2 nanoparticles. But the best result in this category was reported by Hwang et al[7] which demonstrate a stable 907 mA h g^{-1} for 50 cycles at a very high rate of 10.6 A g^{-1} using graphenelike MoS_2 nanoplates. There are few other results reported by Chang et al.[9,10,37] having better electrochemical performance then the present work where in situ carbonization or carbon composite was used to stabilize the MoS_2 electrode. MoS_2/graphene composites[9,37] exhibits stable capacity of 1087 and 1300 mA h g^{-1} for 100 cycles at 100 mA g^{-1} rate, whereas graphenelike MoS_2/amorphous carbon composites[10] exhibits a stable capacity of 912 mA h g^{-1} for 100 cycles at 100 mA g^{-1} rate.

CONCLUSION

The present work emphasizes on few important points, it reports a simple and scalable two-step synthesis process to prepare MoS_2 nanowalls and established the role of binder in the performance of MoS_2 as anode material. Herein, we have also reported the importance of compactness of active material and conductive carbon on the capacity retention. Electrode made of MoS_2 nano walls mixed with carbon and sintered at 700 °C exhibits excellent electrochemical activity when CMC binder was used. A stable capacity of 880 mAh g^{-1} has been achieved at a current rate of 100 mA g^{-1}. The material also exhibits a stable capacity of 676 mAh g^{-1} when discharge at a high rate of 1000 mA g^{-1} and the present result stands ahead than most of the reported results on bare MoS_2 nanoparticles. The excellent electrochemical performance is credited to the following characteristics of 2D-MoS_2 nanowalls structure: (a) the plenty of space between two thin MoS_2 layers, facilitate easy electrolyte diffusion, (b) 2D-wall thickness is in the nano range which again facilitates the solid-state lithium-diffusion in the MoS_2 matrix, (c) the 2D nanowall structure can accommodate huge structural deformation or changes than any other nanostructure, and (d) finally, specific binder-electroactive material−carbon interaction can facilitate the electron percolation as well as hold the conversion reaction products more tightly and more closely. This work successfully establishes the candidature of bare MoS_2 as a high-rate-capable lithium-battery anode and its reported specific capacity value is among the best performances to date.

ASSOCIATED CONTENT

Supporting Information

This material is available free of charge via the Internet at http://pubs.acs.org.

AUTHOR INFORMATION

Corresponding Author

*Fax+91 22 2576 4890. Tel: +91 22 2576 7849. E-mail: sagar.mitra@iitb.ac.in.

Notes

The authors declare no competing financial interest.

ACKNOWLEDGMENTS

We thank "National Centre for Photovolatic Research and Education (NCPRE)"-Ministry of New and Renewable Energy, Government of India and IRCC-IIT Bombay for their support. The authors are thankful to the members of SAIF, IIT Bombay, for their assistance with electron diffraction and FEG-SEM analysis.

REFERENCES

(1) Cabana, J.; Monconduit, L.; Larcher, D.; Palacín, M. R. *Adv. Mater.* **2010**, *22*, E170−E192.
(2) Novoselov, K. S.; Geim, A. K.; Morozov, S. V.; Jiang, D.; Zhang, Y.; Dubonos, S. V.; Grigorieva, I. V.; Firsov, A. A. *Science* **2004**, *306*, 666−669.
(3) Yang, M. C.; Lee, Y.-Y.; Xu, B.; Powers, K.; Meng, Y. S. *J. Power Sources* **2012**, *207*, 166−172.
(4) Cai, J.; Li, Z.; Shen, P. K. *ACS Appl. Mater. Interfaces* **2012**, *4*, 4093−4098.
(5) Li, W.; Yin, Y.-X.; Xin, S.; Song, W.-G.; Guo, Y.-G. *J.Mater.Chem.* **2012**, *22*, 19061−1906.
(6) Cabana, J.; Stoeva, Z.; Titman, J. J.; Gregory, D. H.; Palacín, M. R. *Chem. Mater.* **2008**, *20*, 1676−1678.
(7) Hwang, H.; Kim, H.; Cho, J. *Nano Lett.* **2011**, *11*, 4826−4830.
(8) Das, S. K.; Mallavajula, R.; Jayaprakash, N.; Archer, L. A. *J. Mater. Chem.* **2012**, *22*, 12988−12992.
(9) Chang, K.; Chen, W. *ACS Nano* **2011**, *6*, 4720−4728.

(10) Chang, K.; Chen, W.; Ma, L.; Li, H.; Li, H.; Huang, F.; Xu, Z.; Zhangd, Q.; Lee, J.-Y. *J. Mater. Chem.* **2011**, *21*, 6251−6257.
(11) Zhang, C.; Wang, Z.; Guo, Z.; Lou, X. W. *ACS Appl. Mater. Interfaces* **2012**, *4*, 3765−3768.
(12) Beattie, S. D.; Larcher, D.; Morcrette, M.; Simon, B.; Tarascon, J.-M. *J. Electrochem. Soc.* **2008**, *155*, A158−A163.
(13) Li, J.; Lewis, R. B.; Dahn, J. R. *Electrochem. Solid-State Lett.* **2007**, *10*, A17−A20.
(14) Pan, W. H.; Leonowicz, M. E.; Stieffel, E. I. *Inorg. Chem.* **1983**, *22*, 672−678.
(15) Chang, C. H.; Chan, S. S. *J. Catal.* **1981**, *72*, 139−148.
(16) Windom, B. C.; Sawyer, W. G.; Hahn, D. W. *Tribol. Lett.* **2011**, *42*, 301−310.
(17) Liu, H.; Su, D.; Zhou, R.; Sun, B.; Wang, G.; Qiao, S. Z. *Adv. Energy Mater* **2012**, *2*, 970−975.
(18) Zhang, J.; Wang, Y.; Lin, Z.; Huang, F. *Cryst. Growth Des.* **2010**, *10*, 4285−4291.
(19) Zujovic, Z. D.; Laslau, C.; Bowmaker, G. A.; Kilmartin, P. A.; Webber, A. L.; Brown, S. P.; Travas-Sejdic, J. *Macromolecules* **2010**, *43*, 662−607.
(20) Lei, D.; Zhang, M.; Qu, B. H.; Chen, L. B.; Wang, Y. G.; Zhang, E. D.; Xu, Z.; Li, Q. H.; Wang, T. H. *Nanoscale* **2012**, *4*, 3422−3426.
(21) Gong, J. R., Ed. *Graphene−Synthesis, Characterization, Properties and Applications*. In Tech Open Access Publishers: Rijeka, Croatia, 2011; Chapter 2.
(22) Xiao, J.; Wang, X.; Yang, X.-Q.; Xun, S.; Liu, G.; Koech, P. K.; Liu, J.; Lemmon, J. P. *Adv. Funct. Mater.* **2011**, *21*, 2840−2846.
(23) Dominko, R.; Arcon, D.; Mrzel, A.; Zorko, A.; Cevc, P.; Venturini, P.; Gaberscek, M.; Remskar, M.; Mihailovic, D. *Adv. Mater.* **2002**, *14*, 1531−1534.
(24) Wang, Q.; Li, J. *J. Phys. Chem. C* **2007**, *111*, 1675−1682.
(25) Wang, J.; Yang, J.; Wan, C.; Du, K.; Xie, J.; Xu, N. *Adv. Funct. Mater.* **2003**, *13*, 487−492.
(26) Lestriez, B.; Bahri, S.; Sandu, I.; Roué, L.; Guyomard, D. *Electrochem. Commun.* **2007**, *9*, 2801−2806.
(27) Li, J.; Dahn, H. M.; Krause, L. J.; Le, D. B.; Dahn, J. R. *J. Electrochem. Soc.* **2008**, *155*, A812−A816.
(28) Hochgatterer, N. S.; Schweiger, M. R.; Koller, S.; Raimann, P. R.; Wöhrle, T.; Wurm, C.; Winter, M. *Electrochem. Solid-State Lett.* **2008**, *11*, A76−A80.
(29) Bridel, J. S.; Azaïs, T.; Morcrette, M.; Tarascon, J. M.; Larcher, D. *Chem. Mater.* **2010**, *22*, 1229−1241.
(30) Semmache, B.; Merabet, A.; Gontrand, C.; Laugier, A. *Mater. Sci. Eng., B* **1996**, *38*, 41−45.
(31) Yang, S-w.; Kim, Y. K. *Sol. Energy Mater. Sol. Cells* **2010**, *94*, 2187−2190.
(32) Du, G.; Guo, Z.; Wang, S.; Zeng, R.; Chen, Z.; Liu, H. *Chem. Commun.* **2010**, *46*, 1106−1108.
(33) Feng, C.; Ma, J.; Li, H.; Zeng, R.; Guo, Z.; Liu, H. *Mater. Res. Bull.* **2009**, *44*, 1811−1815.
(34) Xiao, J.; Choi, D.; Cosimbescu, L.; Koech, P.; Liu, J.; Lemmon, J. P. *Chem. Mater.* **2010**, *22*, 4522−4524.
(35) Ding, S.; Zhang, D.; Chen, J. S.; Lou, X. W. *Nanoscale* **2012**, *4*, 95−98.
(36) Zhou, X.; Wan, L.-J.; Guo, Y.-G. *Nanoscale* **2012**, *4*, 5868−5871.
(37) Chang, K.; Chen, W. *Chem. Commun.* **2011**, *47*, 4252−4254.